



Lectures - Wednesday afternoon, June 11

SL19

X-RAY DIFFRACTION SUPPLEMENTED BY MÖSSBAUER AND MAGNETIC MEASUREMENTS OF MECHANICALLY ALLOYED Fe-Al-Mo

P. Roupcová¹, Y. Jirásková²

¹CEITEC - Central European Institute of Technology, Brno University of Technology, Technická 10, 616 00 Brno, Czech Republic

²CEITEC - Central European Institute of Technology, Institute of Physics of Materials, Academy of Sciences of Czech Republic v.v.i., Žitkova 22, 616 62 Brno, Czech Republic
roupcova@ipm.cz

Keywords: ball milling, X-ray diffraction, magnetic behavior, Al-Fe

Abstract

High temperature X-ray powder diffraction measurements were applied to follow the structural and compositional changes in the Fe-Al-Mo samples produced by a high-energy mechanical alloying for various times. The samples after 960 (A), 1920 (B), and 3840 (C) min of alloying using high-energy ball milling were found to embody a different homogeneity. The best result was obtained for B sample with fine-grained structure and homogeneously distributed elements. The X-ray measurements during step-wise increasing temperature from 30 °C up to 1000 °C and the Rietveld analysis of the obtained patterns have confirmed the phase stability of B sample. The X-ray diffractometry is supplemented by magnetic measurements.

Introduction

Fe-Al based alloys form a complete series of solid solutions that are subjected to frequent research efforts. Generally they are interesting materials for their reasonable low cost, low density, high temperature corrosion resistance, good intermediate-temperature mechanical properties, and last but not least the rich variety of magnetic order types observed [1-2]. It is known that by adding ternary transition elements, such as Mo and Ti, not only the high temperature strength but also the magnetic characteristics can be improved. The alloy of Fe – 29 at.% Al – 1.5 at.% Mo composition prepared by conventional technology is known as THERMENOL featured by good soft magnetic properties and high-temperature oxidation resistance [3]. Our effort was to prepare this alloy by high-energy mechanical alloying and to continue a series of alloys prepared by this technology, as Fe-Al [4], and Fe-Mo [5].

Present work is devoted to Fe-Al-Mo system prepared by mechanical alloying into three various states corresponding to three different times of ball milling and to follow changes in the microstructure and chemical composition during thermal treatment using in-situ X-ray measurements. The results are completed by measurements of magnetic properties.

Experimental

Crystalline Fe-, Al-, and Mo-powders of high purity (99.8 %) and particle size below 10 μm were used. The powders corresponding to Fe-29 at.%Al-1.5 at.%Mo composition and summary weight of 30 g were initially mixed in a rotating stainless steel vial without bowl by 200 rpm/2 min. After that 180 g of stainless balls of 10 mm in diameter was added and closed by lid equipped with two needle valves enabling argon purge and creation of the oversaturated Ar atmosphere in the vial. Argon purge was done 1 h initially and after each step of milling when small amount of powder was taken away for further investigation. The milling cycle was set to 10 min of milling at 300 rpm followed by a pause of 5 min. The samples after 960 (A), 1920 (B), and 3840 (C) min were used for next studies.

An X'PertPro diffractometer with CoK_α radiation ($\lambda = 0.17902$ nm) was used for the in-situ studies of the structural changes occurring during temperature treatment. The high temperature measurements were carried out by means of a HTK-1600 heating chamber in a range 30 – 1000 °C in vacuum ($\sim 10^{-2}$ Pa). The powder samples were spread on Pt sample holder. Detailed analysis of powder patterns was realized using the Rietveld structure refinement method and the ICSD database of inorganic and related structures.

The temperature dependences of magnetic moments (thermomagnetic curves) in an external field of 4 kA/m, 4 K/min temperature increase, and the temperature range of 30–800 °C in vacuum ($\sim 10^{-2}$ Pa) were carried out by vibrating sample magnetometer.

Results

The time of ball milling influences significantly the state of an alloying procedure. The A sample milled for the shorter time (Fig. 1) contains besides the bcc-Fe-Al and bcc-Fe-Mo phases still a small amount of Al and Mo, as it follows from the room temperature X-ray pattern analysis. Moreover the peaks corresponding to the Pt sample holder can be seen in all patterns as well. During the step-wise increasing temperature a diffusion of Al and Mo into bcc-Fe proceeds and changes in phase composition are observed. The pattern at 1000 °C is composed mainly of bcc-Fe₇₅Al₂₅ partially transformed into DO₃ and of the bcc-Fe₂AlMo. The finest structure with homogeneously distributed elements was obtained after 1920 min (B) of ball milling

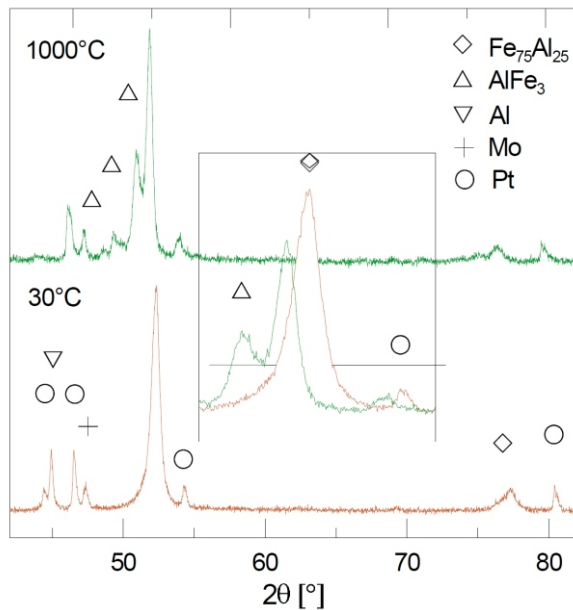


Figure 1. X-ray patterns of A powder sample after ball milling and at 1000 °C.

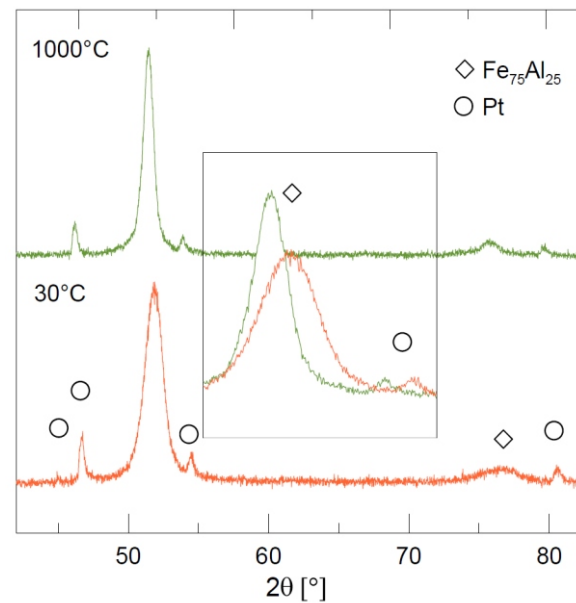


Figure 2. X-ray patterns of B sample after ball milling and at 1000 °C.

which is documented by X-ray diffraction patterns at 30 °C and 1000 °C in Fig. 2. The peak positions correspond to bcc-(Fe,Mo)₇₅Al₂₅ (B2, DO₃) phase. The temperature treatments have contributed to annealing of defects and stresses and slight increase in the mean grain size from 10 nm to approximately (25–30) nm. The next step of milling, sample C in Fig. 3, resulted surprisingly in partial phase decomposition. The pattern obtained at room temperature has embodied again peaks of Mo however they have diminished during annealing and were no more detected at 1000 °C. The patterns of the B and C samples at 1000 °C are not

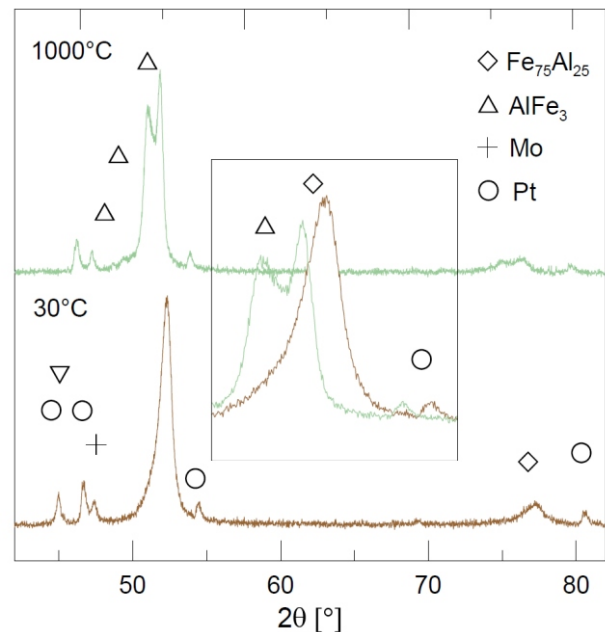


Figure 3. X-ray patterns of B sample after ball milling and at 1000 °C.

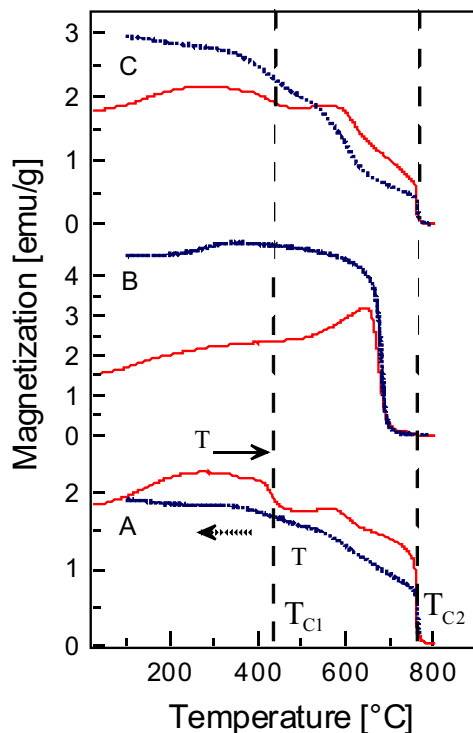


Figure 4. Thermomagnetic curves for A, B, and C samples.

identical. While the B sample consists of mainly (Fe,Mo)₇₅Al₂₅ phase, in the C sample the peaks of Fe₇₅Al₂₅ and Fe₉₆Mo₄ can be resolved.

The thermomagnetic curves depicted in Fig. 4 differ according to a state of alloying and confirm well the results of X-ray diffraction measurements. The initial increase in the mass magnetization is connected with annealing of stresses and defects. It is clearly seen that the B samples is magnetically homogenous and embodies only one Curie temperature close to 690 °C which is in agreement with published value for bcc-(Fe, Mo)₇₅Al₂₅ phase. A somewhat steeper increase in magnetization above approximately 520 °C arises from the DO₃–B2 phase transformation [6]. The Curie temperature T_{C1} detected at A and C samples corre-



sponds to arising bcc-(Fe,Mo)Al phase while the T_{C2} is slightly below the Curie temperature of the pure bcc-Fe.

Conclusion

The in-situ X-ray and magnetic measurements have documented an importance of milling time in an alloying process of the Fe-Mo-Al system. The most structurally and magnetically homogenous sample was obtained after 1920 min of ball milling. The lower time of milling was not satisfactory to obtain required phase homogeneity and the higher milling time has evoked a decomposition of the bcc-(Fe,Mo)₇₅Al₂₅ phase into the bcc-Fe-Al and bcc-Fe-Mo phases. The temperature treatment has led to changes in the phase composition of A and C samples, however both samples at 1000 °C did not result in an identical state from the viewpoint of the composition and the magnetic properties.

SL20

X-ray diffraction as a tool for in-situ monitoring of thermally induced phase transitions

RTG PRÁŠKOVÁ DIFRAKCE JAKO NÁSTROJ PRO IN-SITU MONITOROVÁNÍ PŘÍPRAVY FUNKČNÍCH NANOMATERIÁLŮ

J. Kašlík, J. Filip, Z. Marková, I. Medřík, P. Slovák

*Regionální centrum pokročilých technologií a materiálů, Univerzita Palackého v Olomouci,
17. listopadu 12, 771 46, Olomouc, Česká republika
josef.kaslik@upol.cz*

RTG prášková difrakce patří již dlouhou dobu k nepostradatelným experimentálním technikám materiálového výzkumu. Od jejího objevení a konstrukce prvních difraktometrů prošly přístroje mnoha vývojovými kroky, které umožnily získávat data pomocí RTG práškové difrakce i při jiných než standardních pokojových podmínkách. Jedním z takových příkladů je i RTG difrakce za zvýšených teplot, která v laboratorním měřítku umožňuje in-situ monitorovat průběh reakcí v pevné fázi a reakcí pevná fáze – plyn. Regionální Centrum Pokročilých Technologií a Materiálů (RCPTM) Univerzity Palackého se v několika posledních letech specializuje na vývoj materiálů použitelných pro in-situ remediaci znečištěných, zejména podzemních vod nejen v měřících České republiky, ale i celé Evropy. Při laboratorním výzkumu nových materiálů se právě schopnost sledovat proces termicky indukovaných transformací materiálů přímo v jeho průběhu stala stěžejní pro následný transfer technologie přípravy a optimalizace materiálů do měřítek použitelných pro pilotní aplikace na znečištěných lokalitách.

Materiály vyvíjené pro použití v oblasti čištění vod, případně i dalších environmentálních aplikací, musejí splňovat několik základních vlastností. Pravděpodobně tou nejdůležitější z nich je jejich netoxičita vůči prostředí v němž budou použity. Mezi další důležité vlastnosti patří například finanční nároky na přípravu a skladování, efektivita materiálu a technická a časová náročnost

References

- [1] Schmool, D.S. et al.: *J. Magn. Magn. Mat.*, **272-276** (2004), pp. 1342-1344.
- [2] Ikeda, O. et al.: *Intermetallics* **9** (2001) pp. 755-761.
- [3] Zak, T.: *J. Magn. Magn. Mat.* **41** (1984) pp. 47-48.
- [4] Jiraskova, Y. et al.: *J. Alloys Comp.*, **568** (2013) pp. 106-111.
- [5] Jiraskova, Y. et al.: *J. Supercond. Nov. Magn.* **26** (2013) pp. 1717-1721.
- [6] Nishino, Y. et al.: *Phil. Mag. Lett.* **78:2** (1998) pp. 97-103.

Acknowledgements

The authors thank for financial support the Czech Science Foundation - project P108/11/1350 and the CEITEC – project CZ.1.05/1.1.00/02.0068 (financed by European Regional Development Fund at IPM Brno).

přípravy. Z tohoto důvodu se pro tyto účely začaly vyvíjet materiály tvořené nanočásticemi elementárního železa (nZVI) s různými povrchovými modifikacemi zabraňujícími jejich samovolné prudké degradaci. Materiál tvořený nanočásticemi ZVI kombinuje velmi nízkou hodnotu oxidačně-redukčního potenciálu elementárního železa spolu s velkou aktivní plochou povrchu nanočástic, což jej předurčilo k tomu stát se velmi efektivním pro použití v oblasti reduktivních technologií čištění vod. V současné době jsou již materiály založené na bázi nZVI k čištění vod běžně používány. Vlastní výzkum nových materiálů se ale stále posunuje a do popředí se dostávají kompozitní materiály obsahující nanočástice ZVI imobilizované v/na vhodné matrici. Kompozitní materiály kombinují redukční vlastnosti nanočástic nZVI s výhodnými vlastnostmi použité matrice. Takovou matricí mohou tvořit např. zeolity nebo jílovité minerály, kde se využívá zejména sorpčních vlastností těchto materiálů. Navíc díky magnetickým vlastnostem nZVI lze aplikovaný kompozitní materiál s navázanými polutanty následně magneticky separovat a odstranit z čištěných vod. Další vhodnou matricí pro imobilizaci nZVI mohou tvořit mikročástice železa, jejichž hlavním přínosem je jejich dlouhodobá redukční aktivita.

Při vývoji veškerých výše uvedených materiálů byla do značné míry využita právě vysokoteplotní RTG prášková difrakce, která umožnila velice detailní monitoring vlastních transformačních procesů v průběhu přípravy materiálů a zejména optimalizaci podmínek pro přípravu

materiálu v poloprovodním měřítku. Prezentované výsledky byly pořízeny pomocí vysokoteplotní reakční komůrky XRK900 (Anton Paar, GmbH) nainstalované k difraktometru X'PertPro MPD (PANalytical). Tato reakční komůrka umožňuje provádět experimenty v rozsahu teplot 25 – 900 °C při tlacích plynů v rozmezí 1 mbar až 10 barů ve volitelných reakčních podmínkách (redukční, oxidační, inetrní a další reakční plyny).

Autoři děkují za finanční podporu agentury TAČR (v rámci programu Centra kompetence, projekt č. TE01020218), Ministerstvu Průmyslu a obchodu (v rámci programu TIP, projekt č. FR-TI3/622) a Ministerstvu školství, mládeže a tělovýchovy (v rámci programu Operační program Výzkum a vývoj pro inovace, projekt č. CZ.1.05/2.1.00/03.0058).

SL21

MICROSTRUCTURE EVOLUTION OF TURBOSTRATIC CARBON STUDIED BY DIFFERENT ANALYTICAL METHODS

M. Dopita¹, A. Salomon¹, M. Emmel², C. G. Aneziris² and D. Rafaja¹

¹*Institute of Materials Science, Technical University of Freiberg, Gustav-Zeuner-Strasse 5, Freiberg, D-09599, Germany*

²*Institute of Ceramics, Glass and Construction Materials, Technical University of Freiberg, Agricolastrasse 17, Freiberg, D-09599, Germany
dopita@gmail.com*

A series of high melting synthetic coal-tar pitch Carbores P specimens annealed at different temperatures up to 1400 °C was prepared and the thermally induced microstructural changes were investigated by the combination of different analytical methods. From the structural point of view, the Carbores P is a turbostratic carbon structure, where the individual graphite layers are arranged parallel to each other however with random orientation around the normal to the layers. The temperature evolution of microstructure of investigated samples was studied using the X-ray scattering, neutron scattering, X-ray photo spectroscopy (XPS), Raman scattering, scanning electron microscopy with energy dispersive X-ray spectroscopy (SEM/EDX), transmission electron microscopy particularly with high resolution (TEM/HRTEM) and electron energy loss spectroscopy (TEM/EELS).

The computer program Turbostratic-C, based on the Warren-Bodenstein's theory of scattering on turbostratic carbon allowing fitting of whole measured scattering powder pattern was written and used for refinement of microstructural parameters of studied samples from measured X-ray and neutron scattering patterns. The program enables the refinement of essential physical parameters of turbostratic carbon materials, the mean lattice parameters a_0 , c_0 , mean cluster sizes parallel and perpendicular to the graphitic planes L_a and L_c and its distributions as well as the mean square lattice displacements u_a^2 and u_c^2 .

From X-ray scattering data measured on investigated samples we refined the following, temperature activated, microstructural evolution of the Carbores P. With increasing annealing temperature, the mean cluster size L_a increased from 1.23 nm in initial powder to 6.05 nm in specimen annealed at 1400 °C. This is connected to an increase of the number of atoms in each individual graphitic layer from 46 in the initial powder to 1107 atoms in specimen annealed at 1400 °C. The mean cluster size parallel to graphitic layers increases from 1.07 nm to 4.82 nm, which corresponds to increase of number of layers from 3 to 14 in

initial powder and sample annealed at 1400 °C, respectively. Simultaneously, the width of both distributions increases with growing mean cluster sizes. The evolution of lattice parameter a_0 (the lattice parameter in the graphitic planes, in *ab*-plane) exhibits pronounced increase in samples annealed at temperatures 800 °C and higher. The a_0 lattice parameter changes from $a_0 = 0.2434$ nm in the initial powder to $a_0 = 0.2449$ nm in specimen annealed at 1400 °C. The recalculated in-plane C–C bond length varies from $l_{C-C} = 0.1404$ nm to $l_{C-C} = 0.1414$ nm in raw powder and specimen annealed at 1400 °C, respectively. However, in all investigated specimens the lattice parameters a_0 and the in-plane bond lengths l_{C-C} are smaller than its equilibrium values in undisturbed graphite. Contrary to thermal evolution of lattice parameter a_0 , the lattice parameter c_0 (lattice parameter perpendicular to the graphitic planes, in *c*-direction) decreases with increasing annealing temperature, following well the linear dependence on the annealing temperature. The refined c_0 lattice parameters of turbostratic carbon are in all studied samples higher than those of perfect undisturbed graphite. The lattice parameter c_0 of initial powder is $c_0 = 0.7102$ nm, which is about 6 % more than in unperturbed graphite. With increasing annealing temperatures, the difference between the unperturbed graphitic and turbostratic lattice parameters decreases. In sample annealed at 1400 °C the refined lattice parameter is $c_0 = 0.6883$ nm, which is about 2.6 % higher value than in perfect graphite. The temperature evolution of mean cluster sizes L_a and L_c and lattice parameters a_0 and c_0 are shown in Fig. 1. Using the refined lattice parameters, the X-ray structural density of studied samples was calculated. Calculated densities are smaller than the density of undisturbed graphite, and smallest density $\rho = 2.19$ g/cm³ shows the initial powder. With increasing annealing temperature, the density increases up to roughly 800 °C where it reaches the value of approximately $\rho = 2.23$ g/cm³, which is about 1.5 % less than the density of perfect graphite. The mean square atomic displacements u_a^2 and u_c^2 decreases with

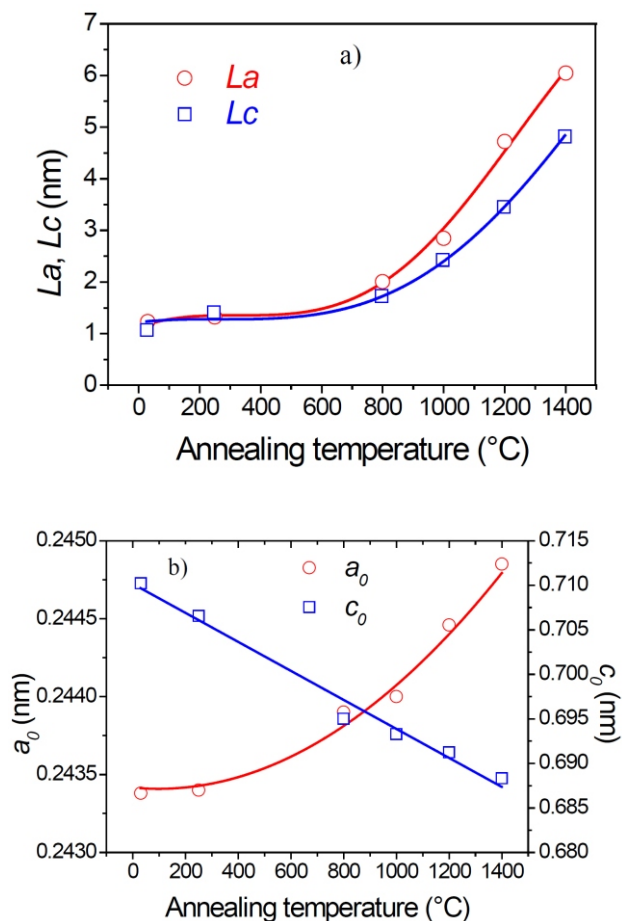


Figure 1. The temperature evolution of the mean cluster sizes parallel and perpendicular to the graphitic planes La and Lc (a). The temperature evolution of the mean lattice parameters in-plane of graphitic layers a_0 , and perpendicular to the graphitic layers c_0 (b), refined from the X-ray scattering data.

increasing annealing temperature, whereas the refined values are in all specimens under study higher than the values of undisturbed graphite. The changes in the refined lattice parameters together with the decay of the mean square atomic displacements, all values tending towards the values of graphite, are attributed to decreasing degree of disorder and concentration of defects with increasing annealing temperature.

The microstructural changes of Carbores P estimated from measured X-ray scattering data were correlated with results obtained from other analytical methods. The evolution of the mean cluster sizes La are in good correspondence with data obtained from the Raman spectroscopy measurements. The information about the bound types and its changes were determined from the XPS and TEM/EELS measurements. The TEM/EELS additionally confirmed the density changes in the annealed samples. The morphological changes of studied samples were investigated using the SEM and TEM. Finally, the changes on the atomic scale, growth of the cluster sizes and decay of the disorder with increasing annealing temperature was confirmed by TEM/HRTEM.

1. B. E. Warren & P. Bodenstern, *Acta. Cryst.*, **18**, (1965), 282.
2. M. Dopita, M. Rudolph, A. Salomon, M. Emmel, C. G. Aneziris & D. Rafaja, *Adv. Eng. Mater.*, **15**, (2013) 1280.

The authors would like to thank the German Research Foundation (DFG) for supporting the subproject A05, which is a part of the Collaborative Research Centre 920 (CRC 920) "Multi-Functional Filters for Metal Melt Filtration - A Contribution towards Zero Defect Materials".

INVESTIGATION OF MICROSTRUCTURE DEFECTS IN HTVPE GROWN POLAR GAN LAYERS

M. Barchuk¹, G. Lukin², C. Röder³, M. Motylenko¹, O. Pätzold², J. Kortus³, D. Rafaja¹

¹*Institute of Materials Science, TU Bergakademie Freiberg, Gustav-Zeuner-Str.5, 09599 Freiberg, Germany*

²*Institute of Nonferrous Metallurgy and Purest Materials, TU Bergakademie Freiberg, Leipziger Str. 34, 09599 Freiberg, Germany*

³*Institute of Theoretical Physics, TU Bergakademie Freiberg, Leipziger Str. 23, 09599 Freiberg, Germany
mikebarchuk@gmail.com*

Gallium nitride (GaN) is a typical representative of the group III nitrides that is widely studied nowadays. Due to the lack of native substrates and high costs for their production, GaN is grown heteroepitaxially on foreign (Al_2O_3 or SiC) wafers. Recently, a successful growth of (0001)-oriented GaN layers by a modified high-temperature vapor phase epitaxy (HTVPE) method on GaN templates was reported [1], which were produced by metal organic chemical vapor phase epitaxy (MOVPE). In contrast to the conventional growth techniques, this inexpensive method employs ammonia (NH_3) and thermally evaporated metallic gallium (Ga) as precursors at atmospheric pressure. However, a significant lattice misfit between the substrate and the GaN template leads to the formation of microstructure defects like threading dislocations (TDs) and stacking faults (SFs).

In this work, we determined the TDs densities in HTVPE GaN layers grown at different ammonia flows on commercial MOVPE-grown GaN templates and compared them with the TDs in the templates. Applying controlled ammonia flow during the growth of particular samples we observed planar defects that can be partial SFs on the (0001)-planes, which are characterized by the absence of nitrogen planes (a or b) in the ...AaBbAaBbAaBb... stack. The residual stress inherent in the heteroepitaxially grown GaN layers is ascertained for all samples under study and MOVPE-GaN templates. The possible reason for the residual stress is the elastic deformation originating both from the lattice misfit and from the interplay between the lattice misfit, differences in the thermal expansion of substrate and GaN and the formation of microstructure defects. The values of the residual stress correlate with the layers thickness and the total density of TDs [2].

A series of three samples (P1-P3) having the thickness of 4.5 μm was grown in a vertical HTVPE reactor [1]. A 2.5 μm thick MOVPE-GaN deposited on the 3-inch c-oriented sapphire substrate was cleaved into the 15x15 mm^2 pieces and used as a substrate for the HTVPE growth. An in-situ deposited SiN_x mask at the initial stages of the MOVPE growth was used to reduce the density of TDs [3]. The growth temperature of all samples was 1080 °C. The ammonia flow, which defines the [N]/[Ga] ratio (V/III ratio), was chosen as a sole variable parameter. In our experiments, the ammonia flow varied between 0.05 and 0.5 standard liter per minute (slm), see Table 1. Additionally, an uncoated piece of MOVPE-GaN template denoted as N1 was investigated.

High-resolution X-ray diffraction (HRXRD), micro-Raman spectroscopy and transmission electron microscopy in scanning mode (STEM) were used as the main experimental techniques in our study.

First, we applied the reciprocal-space mapping in the HRXRD mode in combination with the Monte Carlo approach in order to determine the densities of edge and screw TDs [4]. For this purpose, the symmetrical 004 and the asymmetrical 105 reciprocal-space maps (RSMs) were recorded for each sample. As dislocation bunching is often observed in thicker GaN layers grown by hydride phase epitaxy, a correlation in the dislocation positions must be introduced into the Monte Carlo approach [5]. The results of Monte Carlo simulation shown in Table 1 revealed that the TDs have predominantly edge character. The density of the edge TDs was 4-5 times higher than that the density of the screw TDs. A small decrease of the density of the edge TDs in the HTVPE layers with respect to the MOVPE template was detected for samples P2 and P3 with the low ammonia flow. The density of screw TDs was nearly constant for all samples including the GaN template N1.

In order to determine the residual stress, XRD with a modified \sin^2 method and the micro-Raman spectroscopy were used [2]. The first method recognizes the elastic lattice strain as a shift of the diffraction maxima along the 2 θ direction from their intrinsic positions, whereas the second one detects the strain as a shift of the $E_2(\text{high})$ Raman mode. The X-ray based \sin^2 method determines the averaged strain in the irradiated volume defined by the beam size and the penetration depth. The micro-Raman technique enables to focus the laser beam at a desired depth and to determine the strain locally. The residual stress measurement using both complementary methods is necessary, especially if a depth gradient of the residual stress is expected.

The values of the residual stress are summarized in Table 1. In general, we obtained a good agreement between the XRD and micro-Raman data, with exception of sample P1, where the confocal micro-Raman technique revealed a strong depth gradient of the residual stress. The samples under study possess compressive residual stresses that are comparable with the residual stresses measured in the uncoated MOVPE template. The residual stress in GaN grown on sapphire stems from the lattice misfit and different thermal expansion coefficients of GaN and Al_2O_3 . To some extent, the residual stress results from the uncompensated strain fields of bunched TDs, thus it can be strongly affected by the bunching of the TDs [2].



Table 1. The characteristics of the samples: NH_3 flow (C), density of screw TDs (ρ_s), density of edge TDs (ρ_e), total density of TDs (ρ_{total}), residual stress determined by XRD (σ_{XRD}), averaged over the sample thickness residual stress determined by micro-Raman spectroscopy (σ_{Raman})

Sample	C [slm]	ρ_s [10^8 cm^{-2}]	ρ_e [10^8 cm^{-2}]	ρ_{total} [10^8 cm^{-2}]	σ_{XRD} [MPa]	σ_{Raman} [MPa]
P1	0.5	2.4 ± 0.4	10.3 ± 1.6	12.7 ± 2.0	-608 ± 84	-478 ± 50
P2	0.2	2.0 ± 0.3	7.8 ± 1.2	9.8 ± 1.5	-611 ± 110	-574 ± 50
P3	0.05	2.2 ± 0.3	8.2 ± 1.2	10.4 ± 1.5	-598 ± 65	-585 ± 50
N1	-	2.0 ± 0.3	10.1 ± 1.5	12.1 ± 1.8	-643 ± 83	-650 ± 50

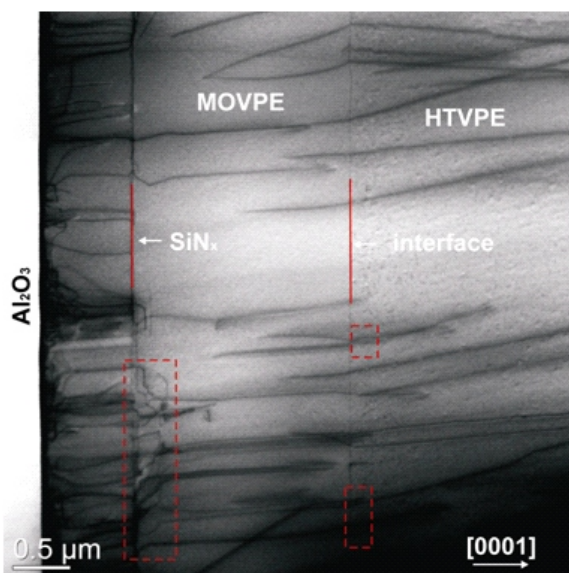


Figure 1. Cross-sectional STEM image of sample P1. The red rectangles refer to the areas where dislocation bunching takes place.

The STEM investigations confirmed the presence of dislocation bunching in the samples (see Figure 1). Here, one can see several areas located close to the interfaces (depicted as red rectangles), where several dislocations converge and form a bunched object. Still, the dislocation lines of the bunched dislocations are oriented nearly perpendicular to the sample surface, i.e., in the $[0001]$ direction.

In sample P3, which was grown under low V/III ratio, the detailed STEM investigations revealed several microstructure defects that deserve our attention (see Figure 2). They are aligned in the basal planes perpendicular to the surface and surrounded by partial dislocations. Unlike the common basal stacking faults (BSFs), these defects do not provide the broadening of the electron diffraction maxima and they do not disappear if the specimen is tilted so that the visibility condition of the BSFs is not fulfilled. If sample P3 is considered as a Ga-rich layer, than the revealed type of planar defects can refer to partial SFs characterized by the absence of nitrogen layers. The investigation of these defects using electron energy loss spectroscopy (EELS) can clarify their nature, whereas the combination of HRXRD with the DIFFaX software [6] can give their quantitative description.

Summarizing, a successful deposition of the low expensive HTVPE GaN layers on the thin MOVPE templates was revealed. The density of TDs in the HTVPE GaN is comparable or even less than the TDs density that can be

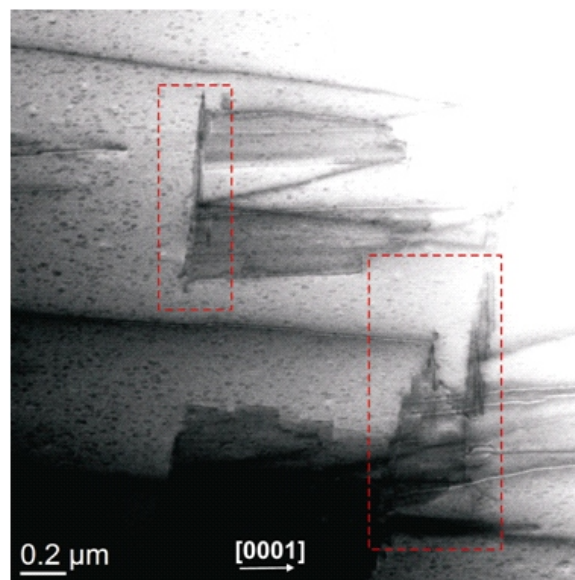


Figure 2. Cross-sectional STEM image of sample P3. The red rectangles mark the areas, which probably contain partial stacking faults terminated by partial dislocations.

achieved in the MOVPE-GaN buffer layer grown by applying the SiN_x nanomask. That makes our method promising for the growth of GaN layers with large thickness. The typical in GaN layers TDs bunching was confirmed by STEM. The compressive residual stress was determined using two techniques. Additionally, planar defects that can probably refer to partial stacking faults were observed in the sample grown under the lowest ammonia flow. The study of their interaction with other defects and the determination of their density will be next steps in our investigations.

1. G. Lukin, C. Röder, M. Barchuk, G. Schreiber, O. Pätzold, J. Kortus, D. Rafaja, M. Stelter, *Phys. Stat. Solidi C*, **11**, (2014), 491-494.
2. M. Barchuk, C. Röder, Y. Shashev, G. Lukin, M. Motylenko, J. Kortus, O. Pätzold, D. Rafaja, *J. Cryst. Growth*, **386**, (2014), 1-8.
3. J. Hertkorn, F. Lipski, P. Brückner, T. Wunderer, S.B. Thapa, F. Scholz, A. Chuvilin, U. Kaiser, M. Beer, J. Zweck, *J. Cryst. Growth*, **310**, (2008), 4867.
4. M. Barchuk, V. Holý, B. Miljevic, B. Krause, T. Baumbach, J. Hertkorn, F. Scholz, *J. Appl. Phys.*, **108**, (2010), 43521.
5. M. Barchuk, C. Röder, J. Kortus, D. Rafaja, *J. Appl. Phys.*, in preparation.
6. M. M. J. Treacy, J. M. Newsam, M. W. Deem, *Proc. Roy. Soc. Lond.*, **A433**, (1991), 499-520.

SL23

STRUCTURAL STUDY OF SrIrO_3 L. Horák¹, X. Martí¹, D. Kriegner¹, C. Frontera²¹Department of Condensed Matter Physics, Charles University in Prague, Czech Republic²Magnetic Materials and Functional Oxides, Institut de Ciencia de Materials de Barcelona, Spain
horak@karlov.mff.cuni.cz

We present a method that allows to determine atom positions in the thin layer epitaxially grown on the substrate whose structure is well known. Usually, the unit cell diameters of the layer and the substrate is very similar which results in the overlap of the diffraction maxima of the layer and the substrate in the reciprocal space. Since, it is not possible to determine the intensity of the layer peak, and consequently, to determine the atomic positions from the structure-factor amplitude. On the other hand, the knowledge of the atomic arrangement in thin strained layers is very important as it is related to the material properties which can be diametrically different from those in a bulk.

The measured diffraction curve along the crystal truncation rod is a result of the interference between the wave diffracted in the substrate and in the layer. From the atomic arrangement in the substrate unit cell, which is usually well-known for the bulk single crystal, it is possible calculate exactly the diffracted wave by the substrate. We use the

dynamical theory of diffraction to calculate the diffraction curve [1]. Here, the known substrate wave serves as a reference and the atomic arrangement in the layer is refined to fit the experimental data.

We demonstrated this method on a set of epitaxial layers of SrIrO_3 grown on different substrates (DyScO_3 , NdScO_3 , GdO_3). Several tenths of the diffractions for each sample were measured and all experimental data were simultaneously fitted. The first guess was derived from the structure of the substrate as all materials in this class have a similar atomic arrangement and the same space group (Pnmb). From the fitting we were able to refine atomic arrangement. The sensitivity of this method is demonstrated by the figure bellow which shows that the interference pattern significantly differs for the guessed (started) arrangement and for the refined one.

1. Pietsch, U., Holý, V. and Baumbach, T., *High-resolution X-ray Scattering from Thin Films to Lateral Nanostructures* (New York: Springer), 2004.

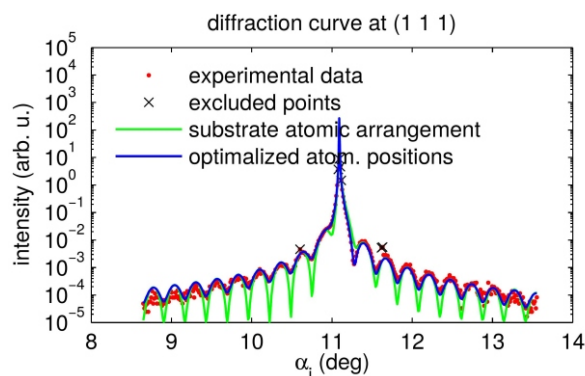
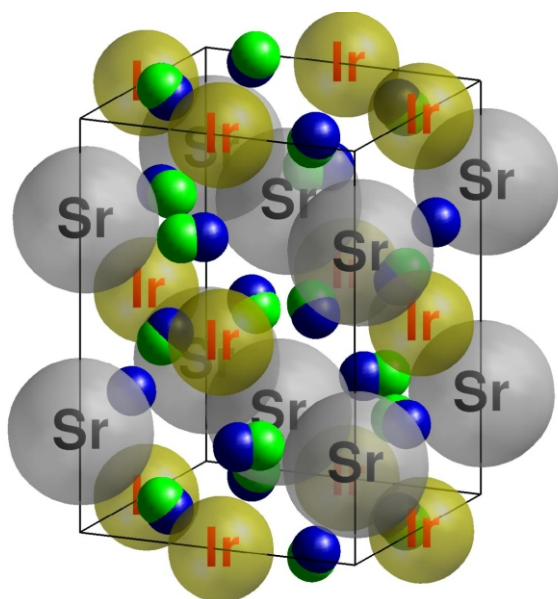


Figure 1. On the left, there is shown the unit cell of SrIrO_3 (sp.gr. Pnmb) simultaneously for both considered atom configurations: the substrate-like atomic arrangement and the refined atomic arrangement. The positions of the heavy atoms are very similar for both cases whereas the positions of the oxygen atoms differ. Their positions are indicated by the green (substrate-like) and blue spheres (refined arrangement). The plot on the right shows the diffraction curve measured (red points) at $\text{SrIrO}_3/\text{NdScO}_3$ (111) diffraction maxima. We simulated the diffraction curve based on the substrate-like (green curve) and the refined (blue curve) atomic arrangement.